Journal of Membrane Science 457 (2014) 162–169

Contents lists available at ScienceDirect

Journal of Membrane Science

journal homepage: www.elsevier.com/locate/memsci

# Hydrophilic nylon 6,6 nanofibers supported thin film composite membranes for engineered osmosis

Liwei Huang, Jeffrey R. McCutcheon *

*University of Connecticut, Department of Chemical and Biomolecular Engineering, Center for Environmental Sciences and Engineering, 191 Auditorium Rd., Unit 3222, Storrs, CT 06269-3222, USA*

ARTICLE INFO

*Article history:*
Received 27 October 2013
Received in revised form
13 January 2014
Accepted 18 January 2014
Available online 25 January 2014

*Keywords:*
Nylon 6,6
Electrospinning
Nanofibers
Forward osmosis
Interfacial polymerization

ABSTRACT

Previous studies have concluded that an ideal thin film composite (TFC) membrane specially designed for Engineered Osmosis (EO) should have an ultra-thin selective layer with excellent permselectivity supported by a hydrophilic, highly porous, non-tortuous and thin support structure. In this study, an emerging TFC supporting material, electrospun nanofibers, were used to fabricate a TFC-EO membrane where the support structure and the selective layer properties were individually optimized. Specifically, nylon 6,6 nanofibers fabricated via electrospinning were used for the first time to form the support structure due to its intrinsic hydrophilicity and superior strength compared to other nanofiber materials. The resulting membrane exhibited half of the structural parameter of a regularly used commercial FO membrane. Furthermore, the selective layer permselectivity could be adjusted using a co-solvent during the interfacial polymerization processes. Adding acetone to the organic phase (hexane) was found to increase permeance and decrease selectivity and hence affect the osmotic flux performance of our membranes. Our best membrane outperformed the standard commercial FO membrane by exhibiting a 1.5 to 2 fold enhanced water flux and an equal or lower specific salt flux.



## 1. Introduction

Engineered Osmosis (EO) is an emerging platform technology that harnesses the natural phenomenon of osmosis to address water and energy scarcity [1–3]. In this process, an osmotic pressure difference is generated when two solutions of differing concentration are placed on two sides of a semi-permeable membrane. This difference drives the permeation of water across the membrane from the dilute solution to the concentrated solution. The potential of this technology has been demonstrated in a variety of applications, such as forward osmosis (FO) for seawater desalination [4–7], pressure retarded osmosis (PRO) for electric power generation [8–11], and direct osmotic concentration (DOC) for recovering high-value solutes [12–14]. However, EO processes have not yet become commercialized on a large scale. One major obstacle is the lack of a membrane specifically designed for any of these processes [15–18].

Recently, aromatic polyamide thin film composite (TFC) membranes have become more common as a platform EO membranes. They have begun to replace more conventional asymmetric integral membranes in both flat-sheet [15,17–20] and hollow fiber forms [16,21,22] due to their superior permselectivity. Furthermore, TFC membranes are more flexible in their design as both the selective and support layers can be independently tailored. While this flexibility accelerated the widespread adoption of reverse osmosis (RO) [23]. Membranes designed for EO must have specific, these membranes performed poorly during early work on the development of osmotic processes [5,24,25]. The hydrophobic cast polysulfone (PSu) support layer and the thick nonwoven fabric baking layer of a conventional TFC membrane [26–28] cause severe mass transfer resistance near the interface of the selective thin film layer. This phenomenon, widely described as internal concentration polarization (ICP), reduces effective osmotic driving force and results in poor water flux performance [5,25,29–31].

Membranes tailored for EO must be designed based on specific criteria related to their structure and chemistry. The selective layer must have excellent permeance and selectivity. The support layer must be thin and have a highly porous and interconnected (low tortuosity) structure. The support layer must also be hydrophilic, allowing for complete saturation (i.e. wetting) throughout the structure [32]. Lastly, the membrane as a whole must exhibit excellent chemical and thermal stability while retaining reasonable mechanical strength.

In our previous study, we demonstrated the fabrication of a novel TFC membrane based on a commercially-available hydrophilic nylon 6,6 microfiltration membrane [33]. This TFC membrane exhibits

* Corresponding author. Tel.: +1 860 486 4601.
*E-mail address:* jeff@engr.uconn.edu (J.R. McCutcheon).

0376-7388/$ - see front matter © 2014 Published by Elsevier B.V.
http://dx.doi.org/10.1016/j.memsci.2014.01.040

higher flux and selectivity compared to a commercially available FO membrane despite the fact that it has a structural parameter 3 times higher than that membrane (about 2000 μm). The improved performance can be attributed to the relatively good permselectivity of the polyamide film coupled with hydrophilicity of the support. We hypothesized that the performance could be further improved by reducing the structural parameter. This can be achieved by replacing this cast support with a thinner, more porous, and less tortuous nylon 6,6 structure.

Electrospun nanofibers are a class of material that exhibits an intrinsically high porosity with an interconnected pore structure. These unique features make nanofiber mats promising candidates for TFC-EO membrane supports. Recently, a few studies have been reported on designing TFC-EO membranes based on PSu [20], polyethersulfone (PES) [20,34], polyacrylonitrile (PAN) [35], Polyvinylidene fluoride (PVDF) [36] and PAN/cellulose acetate (CA) blends as an electrospun nanofiber support [37]. High osmotic flux and low structural parameters were achieved for these membranes as a result of the intrinsically high porosity and low tortuosity of the nanofiber mats. Despite the promising flux performance of this new class of TFC-EO membrane, the potential of nanofiber based TFC membranes has not been fully developed considering the large number of materials that are spinnable and post-modifications that can further improve the properties of the nanofibers.

This study introduces a novel type of flat-sheet polyamide TFC membrane supported by a nonwoven web of nylon 6,6 nanofibers spun onto a commercial nonwoven fabric. Nylon 6,6 polymer is a suitable material as a nanofiber support considering its intrinsic hydrophilicity, good mechanical properties, and excellent compatibility with a polyamide selective film [33]. The polyamide selective layer was polymerized in situ onto the nanofiber support using interfacial polymerization (IP). This method is commonly applied in fabricating RO membranes, We have modified the method using the approach reported by Kong et al. [38] referred to as co-solvent assisted interfacial polymerization (CAIP) where a co-solvent (acetone) (Ac) was added to a nonpolar organic (hexane) phase to form a miscibility zone in the hexane/water/acetone system. When a co-solvent is added the reaction zone is changed because of the change in miscibility of the two solutions at the interface. By changing the amount of acetone, we can adjust the permselectivity of the polyamide layer over a wide range. This CAIP approach would help us to understand the support-selective layer interactions as well as structure–performance relationships for this new nanofiber support based TFC-EO membranes. Knowledge of these relationships will provide valuable insight into designing future TFC membranes with low structural parameter supports.

## 2. Experimental

### 2.1. Materials

Nylon 6,6 ($M_W$ 262.35), Dichloromethane (DCM, anhydrous, >99.8%), m-phenylenediamine (MPD, >99%) and trimesoyl chloride (TMC, 98%) were purchased from Sigma-Aldrich (St. Louis, MO). Formic acid (FA, 88%, Laboratory), hexane (HPLC, >98.5%), Acetone (Ac, certified ACS) and sodium chloride (NaCl, crystalline, certified ACS) were purchased from Fisher Scientific (Pittsburgh, PA). Deionized water (DI) was obtained from a Milli-Q ultrapure water purification system (Millipore, Billerica, MA). Commercial asymmetric cellulose triacetate (HTI-CTA) FO membrane (Hydration Technology Innovations Inc., Albany, OR) were acquired for comparison and these membranes were designated as HTI hereafter. Polyester nonwoven fabric sheet (PET, Novatexx 2442) was supplied by Freudenberg (Weinheim, Germany). The thickness of the PET nonwoven is approximately 60 μm.

### 2.2. Electrospinning nylon 6,6

FA is a commonly used solvent for preparing nylon 6,6 electrospinning solution [39–41]. However, our preliminary work shows that nylon 6,6 dissolved in FA is relatively difficult to spin probably due to the fact that FA has a relatively low vapor pressure. In this study, DCM, a low-boiling point and inexpensive solvent was blended with FA to increase the solvent evaporation rate [42]. The best ratio of FA and DCM solvents was found to be 8:2 in order to facilitate fiber spinning while still maintaining reasonable adhesion between the electrospun nonwoven midlayer and the PET backing layer [43–46]. Higher ratio of DCM might result in nanofibers drying before depositing onto the PET, preventing good adhesion to other deposited fibers or to the PET substrate. Higher ratio of FA, on the other hand, might not yield high quality fibers or might results in fibers dissolving after deposition.

The nylon 6,6 electrospinning parameters are summarized in Table 1. Nylon 6,6 pellets were mixed in a co-solvent mixture of FA and DCM overnight under room temperature to obtain 10 wt% homogeneous solution. A volume of 2.5 mL of this solution was electrospun onto the PET backing layer under a potential field of 25 kV to form a nanofibrous mat. The experiments were conducted at ambient temperature and humidity using a system described in our previous study [20,45]. Under the selected spinning conditions, nylon 6,6 could be spun easily, producing high-quality fibers with very few defects and beads.

### 2.3. Polyamide formation

Both conventional IP and CAIP were employed to form polyamide selective layers onto the nylon 6,6 to fabricate the TFC membranes. The conventional IP process is as follows. First, the nylon 6,6 nonwoven mats spun onto a PET were taped onto a glass plate with the nanofibers facing up. The nanofiber-PET support was immersed into a 1.0% (wt/v) aqueous MPD solution for 120 s. Excess MPD solution was removed from the support membrane surface using an air knife. The nanofiber supports were then dipped into a solution of 0.15% (wt/v) TMC in hexane for 60 s to form an ultrathin polyamide film. The resulting composite membranes were subsequently cured in an air-circulation oven at 70 °C for 10 min to attain the desired stability of the formed structure. The TFC polyamide membranes were thoroughly washed and stored in DI water at 4 °C.

The CAIP membranes were prepared using the same process with Ac co-solvent added into the TMC/hexane organic phase.

**Table 1**
Summary of electrospinning conditions for nylon 6,6 nanofibers support.

| Conditions | |
|---|---|
| **Polymer** | Nylon 6,6 |
| **Solvent** | 80% FA/20% DCM |
| **Concentration** | 10 wt% |
| **Voltage** | 28 kV |
| **Flow rate** | 0.8 ml/hr |
| **Tip-to-target distance** | 8 cm |
| **Drum rotating speed** | 30 rpm |
| **Total volume of solution** | 2.5 ml |
| **Area of the collector surface** | 90 $cm^2$ |

The hexane solution of TMC and acetone was prepared as follows. First, an amount of TMC was completely dissolved in the hexane solution and the resulting solution was continuously stirred for 2–3 h. Then a certain amount of acetone was added (0.75–4% (v/v)), followed by stirring for 30 min.

The resulting TFC membranes based on IP were designated as TFC-0. Membranes formed using CAIP containing Ac 0.75%, 2.0%, and 4.0% were referred to TFC-0.75, TFC-2, and TFC-4, respectively.

### 2.4. Membrane characterization

Surface morphology and cross-sectional structure of the nylon 6,6 nanofiber support and the composite membranes (both based on IP and CAIP) were characterized with scanning electron microscopy (SEM) using a cold cathode field emission scanning electron microscope JSM-6335F (FEI Company, USA). Before imaging, samples were kept overnight in a desiccator and then sputter coated with a thin layer of platinum to obtain better contrast and to avoid charge accumulation. For cross-sectional imaging, PET backing layer was first removed followed by freeze-fracturing the sample using liquid nitrogen to obtain a clean edge with preserved structure. ImageJ software was used to determine the average fiber diameter and fiber diameter distribution by measuring 20 different fibers.

Water contact angles on the nanofibrous support surface were measured using the sessile drop method on a CAM 101 series contact angle goniometer (KSV Company Linthicum Heights, MD). The values were taken as an average of at least five points with a volume of $10 \pm 1$ μL.

A Millipore Amicon bioseparations stirred cell (model 8200, Fisher scientific, Pittsburgh, PA) with active filtration area of 28.7 $cm^2$ was used to evaluate the pure water permeance of the nylon 6,6 nanofiber support (with the PET layer attached). A hydraulic pressure of 10 psi was applied to the cell.

The mechanical properties of as-spun nanofibrous mats and the TFC-no-PET membranes were obtained from the tensile tests in air at 25 °C using an Instron microforce tester. A dynamic mechanical analysis (DMA) controlled force module was selected and the loading rate was 0.5 N/min. A minimum of three strips of length 40 mm × 5.5 mm were tested from each type of membrane. The PET backing layers were removed prior to tests for all samples. Tests were also conducted on wetted samples by wetting the samples after they were loaded into the instrument.

### 2.5. Membrane performance tests

#### 2.5.1. Reverse osmosis tests to determine membrane permeability coefficients

A bench-scale cross-flow RO testing unit was used to evaluate the intrinsic pure water permeance, $A$, observed salt rejection, $\%R$, and solute permeability, $B$, of the TFC membranes at $20 \pm 1$ °C using a method described elsewhere [33]. The system was operated at 100 psi with a fixed cross-flow velocity of 0.13 m/s (Re ~ 600) using DI or a 2000 ppm NaCl feed solution to determine $A$ and $\%R$, respectively. The PET backing layer was attached during the RO tests.

#### 2.5.2. Osmotic flux tests and determination of TFC membrane structural parameters

Osmotic water flux and reverse salt flux of the TFC IP and CAIP membranes were evaluated using a custom lab-scale cross-flow forward osmosis system. The experimental setup was described in details elsewhere [47]. A 1.0 M NaCl solution was used as the draw solution while DI water was used as the feed solution. Osmotic flux tests were carried out with the membrane oriented in both PRO mode (the membrane active layer faces the draw solution) and FO mode (the membrane active layer faces the feed solution). The hydraulic pressures of the feed and draw solutions were the same (1.5 psi) and the cross-flow velocities were kept at 0.13 m/s for both the feed and draw solutions. The temperatures of the feed and draw solutions were maintained at $20 \pm 1$ °C using a recirculation water bath and a heat exchanger. Membranes were tested with the PET backing layers attached.

The osmotic water flux, $J_w$, was calculated by dividing the volumetric flux by the membrane area. By measuring the conductivity of the feed solutions at certain time points during the tests, the reverse salt flux, $J_s$, was calculated by dividing the NaCl mass flow rate by the membrane area. The specific salt flux is a simply a ratio of salt flux to water flux, $J_s/J_w$. The structural parameter was determined by using the equation [15] where the membrane is orientated in FO mode:

$$S = \left(\frac{D}{J_w}\right)\left(\ln\frac{B + A\pi_{D,b}}{B + J_w + A\pi_{F,m}}\right) \quad (1)$$

In this equation, $D$ is the diffusion coefficient of the draw solute, $J_w$ is the measured water flux, $B$ is the solute permeability, $A$ is the water permeance, $\pi_{D,b}$ is the bulk osmotic pressure of the draw solution, and $\pi_{F,m}$ is the osmotic pressure at the membrane surface on the feed side (0 atm for DI feed). This model is only valid with the following major assumption: (1) the membrane reflection coefficient is assumed to be 1; (2) the external concentration polarization (ECP) of the draw side is negligible when compared to ICP; (3) ECP of the feed side is neglected due to the use of DI water as feed and low reverse salt flux [48]. Assumption (1) and (3) imply that this model is only valid for tight salt rejecting membranes.

This standard method for determination of structural parameter involves fitting the intrinsic membrane properties $A$ and $B$ that determined in RO into the model. However, recently a new methodology for simultaneously determination of $A$, $B$ and $S$ only by means of FO experiment has been reported. The values of $A$ and $B$ obtained by the FO method were systematically different than those obtained by the standard approach [48]. Nevertheless, we still chose the standard approach to evaluate $S$ in order to better compare the membrane parameters with literature using the existing method.

## 3. Results and discussion

### 3.1. Nanofibers morphology and hydrophilicity

The surface morphology of the nylon 6,6 nanofiber nonwoven is shown in Fig. 1(a). Uniform and bead-free fibers with both cylindrical and ribbon-like morphology were obtained. The formation of ribbons is explained by the fast evaporation of the solvent during the electrospinning process that leads to the formation of a solid skin that shrinks and collapses upon the evaporation of the remaining solvent [42]. The average diameter of the fibers is approximately 270 nm. Fig. 1(b) shows a Gaussian-like distribution between 100 and 400 nm, though few ribbon-like fibers fall into 600–700 nm range. Note that relatively uniform and small fibers will result in an ENS with consistently small pore sizes [49], which may better support the polyamide selective layer [50,51]. The contact angle of the fiber mat surface is measured to be approximately 38° (Fig. 1(c)), indicating the hydrophilicity of the nanofiber support. This result is consistent with the contact angle of a nylon 6,6 phase-inversion microfiltration membrane (40.5°) [33]. The pure water permeance of the nylon 6,6 nanofiber support is measured to be $7632 \pm 177$ LMH/bar.

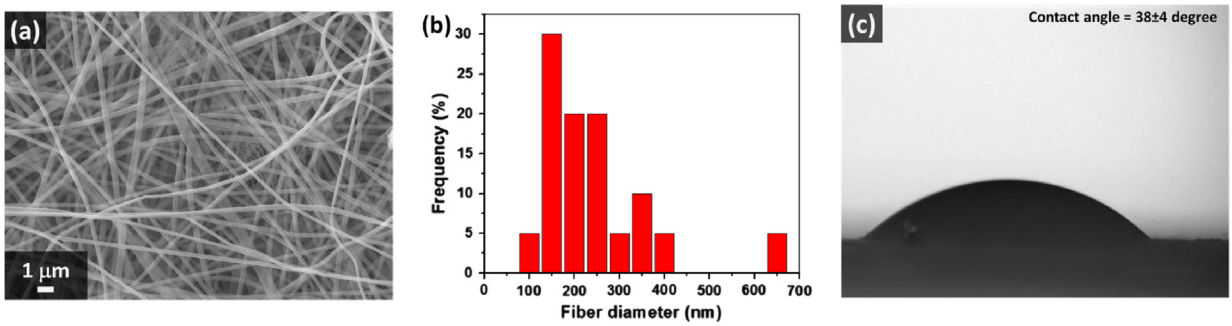


**Fig. 1.** Properties of e-spun nylon 6,6 nanofiber support. (a) Top surface SEM micrographs; Magnification: 5000×. (b) Fiber diameter distribution. Nanofibers have an average diameter of 270 ± 120 nm. (c) Contact angle of the top surface.

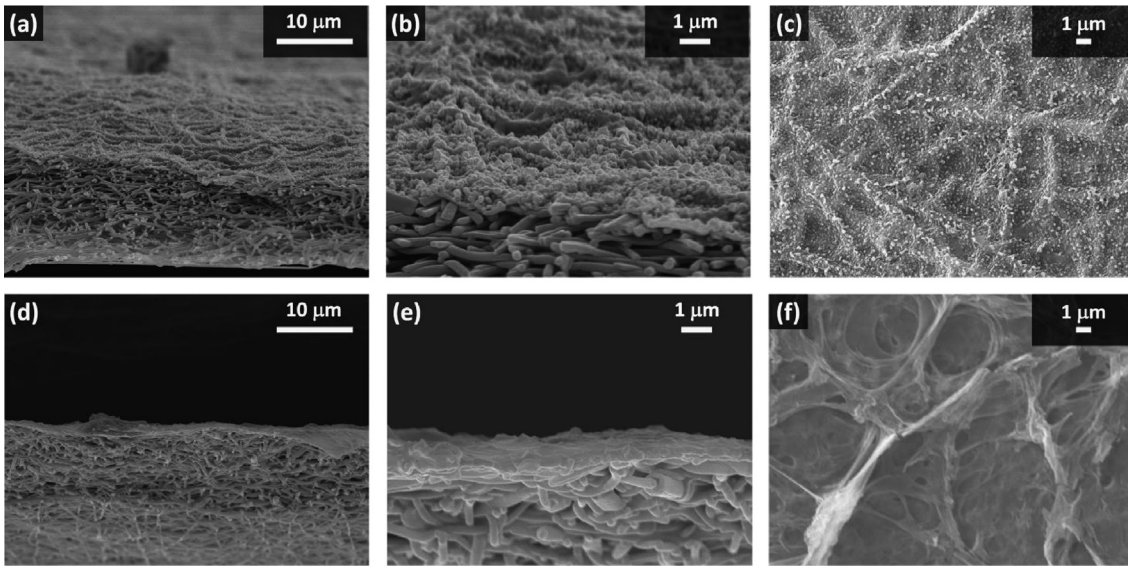


**Fig. 2.** (a) Cross-sectional micrographs of conventional IP TFC membrane (TFC-0); Magnification: 2500×. (b) Higher magnification (10,000×) of (a). (c) Top surface micrographs of polyamide selective layer of conventional IP TFC membrane (TFC-0); Magnification: 5000×. (d) Cross-sectional micrographs of CAIP TFC membrane (TFC-2); Magnification: 2500×. (e) Higher magnification (10,000×) of (c). (f) Top surface micrographs of polyamide selective layer of CAIP TFC membrane (TFC-2); Magnification: 5000×.

### 3.2. TFC microstructure and surface morphology

The cross-section microstructure and surface morphology of both IP and CAIP membranes are shown in Fig. 2. The total thickness of both the IP and CAIP composite membranes without the PET were between 8 and 10 μm, as estimated using both SEM (Fig. 2(a) and (d)) and a micrometer. The overall thicknesses of the TFC membranes with the PET layers were approximately 70 μm. Higher magnification SEMs (Fig. 2(b) and (e)) show different interactions between the polyamide film and the nanofibers for IP and CAIP membranes. The polyamide layer of the IP-TFC seems to directly integrate with the first nanofiber layer, while the polyamide film of the CAIP-TFC appears to merely sit on top of the ENS. Further, the IP-TFC gives the characteristic peak-and-valley polyamide structure. However, this "globular morphology" was not seen on the CAIP-TFC membrane. This difference is further evidenced by the top-surface SEM images (Fig. 2(c) and (f)). A denser surface of the polyamide film was obtained for IP-TFC which looks like an imprint of the nanofibers underneath. However, a less dense surface was formed for CAIP-TFC which entirely covers the nanofiber feature of the support. This result is consistent with previous study on CAIP [38]. Freger [52] theoretically predicted that a narrow reaction zone appeared at the initial stage of conventional IP process since there is an immiscibility gap in the hexane/water binary system and the reaction only occurs at the liquid–liquid interface. In the CAIP system, the interfacial tension and solubility differences are greatly decreased due to the miscibility zone exhibited in hexane/water/acetone ternary system, which possibly leads to better partitioning of MPD into the organic phase and broadening of the reaction zone. Therefore, a looser, less dense polymer layer was achieved.

### 3.3. Mechanical properties of ENS and TFCs

In the case of EO, the support of the TFC membrane should be designed to exhibit low structural parameter yet still keep necessary strength in order to withstand osmotic water flow. Membranes for PRO must also be capable of tolerating of at least 12–13 bar if not higher for osmotic engine applications. In addition, membranes should have enough strength for ease of manufacturing, processing and handling. For instance, membranes should maintain enough flexibility so that they can be assembled into a module. Tensile strength test might be a good indicator on flexibility and handleability of the material. It may also give us some insight on membrane tolerance to operating conditions. It is well known that nanofiber mats have poor tensile strength largely a result of low individual fiber strength, a high porosity, and poor bonding between the fibers. Table 2 compares the tensile strength of nylon 6,6 nanofibers with those of other polymers reported in literature which are commonly used as membrane materials

**Table 2**
Summary of tensile strength of nanofibers of polymers commonly used as TFC support materials.

| Support platform | Materials | Abbreviation | Tensile strength (MPa) | Reference |
|---|---|---|---|---|
| **Nanofibers** | **Nylon 6,6** | N/A | 10.0 | This work |
| | **Polyethersulfone** | PES | 1.8 | [43] |
| | **Polysulfone** | PSu | 0.8 | [46] |
| | **Polyacrylonitrile** | PAN | 5.7 | [46] |
| | **Cellulose acetate** | CA | 1.2 | [53] |
| | **Polyvinylidene fluoride** | PVDF | 2.0 | [54] |
| | **Polyethersulfone** | PES | 5.5 | [55] |
| **Phase-inversion cast film** | **Polysulfone** | PSu | 7.3 | [56] |
| | **Polyacrylonitrile** | PAN | 4.5 | [57] |

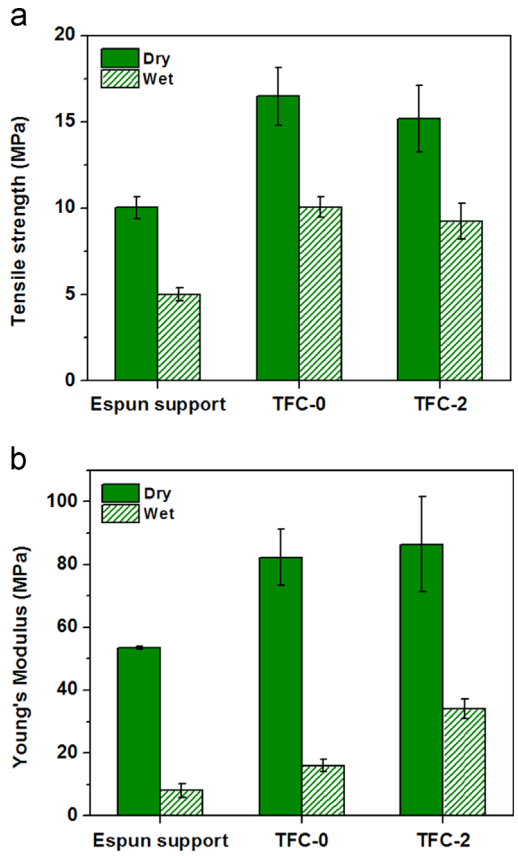


**Fig. 3.** Mechanical properties of E-spun PA 6,6 support, conventional IP TFC membrane (TFC-0) and CAIP TFC membrane (TFC-2): (a) tensile strength. (b) Young's Modulus.

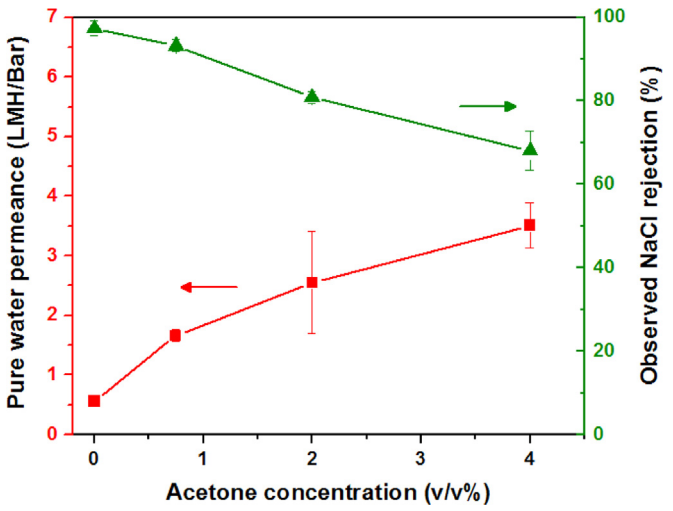


**Fig. 4.** Pure water permeability coefficient and observed rejection of CAIP TFC membranes prepared with different acetone concentrations. Experimental conditions: 20 ± 1 °C; DI water and 2000 ppm NaCl as the feed solution for measuring pure water permeability coefficient and rejection, respectively; cross-flow velocities of 13.18 cm/s (Re ~ 600).

[43,46,53,54], as well as some conventional phase-inversion casting materials [55–57]. As seen in Table 2, we achieved a relatively strong fiber support by spinning nylon 6,6 compared to other nanofibers. Its strength is even comparable to conventional phase-inversion supports. We believe the superior strength of nylon 6,6 may be a results of the intrinsic properties of nylon 6,6 polymer. Nylon 6,6 is known for its highly crystalline structure due to strong intermolecular hydrogen bonding between parallel polymer chains which can form multi-chain sheets and a strong and tough supermolecular structure. The relatively high strength of nylon 6,6 nanofibers may make it desirable as a TFC-EO membrane support.

Fig. 3 represents the mechanical properties of the as-spun nylon 6,6 fibers (without PET) and the TFC membranes based on both conventional IP (TFC-0) and CAIP (TFC-2). It can be seen that both IP-TFC and CAIP-TFC have higher strength and modulus than the as-spun fibers. This increase can be attributed to the integration of the nanofibers into the polyamide layer to form a "composite structure", transferring higher strength and rigidity of polyamide layer to the relatively weak nanofibers. Bui et al. observed the similar phenomenon on nanofiber based TFC membranes [37]. IP-TFC seems to have slightly higher strength but lower modulus than the CAIP-TFC. This is due to the higher crosslinking in the IP-TFC selective layer which is stronger and stiffer than the more open, thicker CAIP polyamide layer.

Many membrane strength tests are done when the membrane is dry. However, this is not necessarily indicative of the membrane properties when it is in operation. We therefore also tested these membranes in their wet state. Upon wetting, there is a dramatic decrease in both strength and modulus for both nanofiber mats and the TFC membranes. We attributed this decrease to swelling of the hydrophilic nanofibers which can compromise the mechanical integrity of the support as well as the composite structure. We believe this issue to be universal for most intrinsically hydrophilic nanofibers due to their high porosity and surface area. Though hydrophilicity is a desirable feature for EO membrane supports, swelling might become a major challenge for liquid based applications of hydrophilic nanofibers.

### 3.4. Performance of TFC membranes

#### 3.4.1. Permselectivity of polyamide selective layers

Our IP-TFC and CAIP-TFC membranes were tested in cross-flow reverse osmosis using the HTI CA membranes as a control. Fig. 4 shows water permeance and observed rejection for a 2000 ppm NaCl solution with both types of TFC membranes as a function of

**Table 3**
Summary of pure water permeance ($A$) and solute permeability ($B$) of HTI and TFC membranes based on IP and CAIP conditions. *Experimental conditions*: 2000 ppm NaCl feed solution, cross-flow velocity of 0.13 m/s, and temperature of 20 °C.

| Membranes | $A$ (LMH/bar) | $B$ (LMH) |
|---|---|---|
| **HTI** | $0.57 \pm 0.03$ | $0.17 \pm 0.02$ |
| **TFC-0** | $0.56 \pm 0.04$ | $0.05 \pm 0.04$ |
| **TFC-0.75** | $1.66 \pm 0.10$ | $0.54 \pm 0.13$ |
| **TFC-2** | $2.55 \pm 0.86$ | $1.37 \pm 0.35$ |
| **TFC-4** | $3.51 \pm 0.38$ | $4.12 \pm 1.29$ |

Ac concentration in hexane solutions. With increasing Ac concentration from 0% to 4%, water permeance increased up to 7-fold (from 0.56 to 3.51 LMH/bar) while rejection decreased from 97.4% to 68.1%. Results indicated that by employing CAIP approach, we achieved a series of TFC membranes with a wide range of permselectivity difference. The use of these different membrane allowed for the first systematic study on effect of permselectivity on osmotic flux performances of nanofiber supported TFC membranes. The use of Ac as a co-solvent is effective in tuning permselectivity because, as described above, Ac will broaden the miscibility region formed at the interface, which leads to a wider and looser reaction zone. The resulting membranes have a lower cross-link density and thus a lower selectivity but higher permeability. It is also worth noting that the nanofiber-supported TFC membranes were still able to withstand an applied hydraulic pressure of at least 100 psi even though mechanical strength tests revealed that the integrity might be compromised when membranes were exposed to water.

Table 3 summarizes the pure water permeance, $A$, and NaCl permeability, $B$, of the HTI membrane alongside our TFC membranes. Our conventional IP membrane (TFC-0) exhibited more than 3 times lower $B$ than the HTI membrane, indicating higher selectivity. However, both the HTI and our conventional IP membrane suffered from low water permeance. Our CAIP membranes (TFC-0.75, 2, and 4), on the other hand, are more permeable and less selective than HTI.

### 3.4.2. *Osmotic flux performance of TFC membranes*

The osmotic water fluxes and reverse salt fluxes of the membranes are presented in Fig. 5(a) and (b), respectively. With increasing Ac concentration in hexane, water flux increased and then gradually decreased for both the FO and PRO modes. TFC-0.75 achieved the highest water flux while TFC-4 exhibited the worst performance among the four TFC membranes. Meanwhile, the reverse salt flux of our TFC membranes increased considerably with increasing Ac concentration due to reduced selectivity of the membranes. Since all four membranes were fabricated upon the same support, the difference in osmotic water flux can be only attributed to the difference in permselectivity of the polyamide selective layers. Compared to TFC-0.75, TFC-0 suffers from a low permeance and hence low water flux. For TFC-4, the lower water flux performance is attributed to the substantially higher $B$ values, which lead to more reverse salt permeation, as can be seen in Fig. 5(b). The loss of osmotic pressure difference overwhelms the benefit of higher water permeance. Furthermore, the reverse salt permeation also induces ICP in the PRO mode. The result is consistent with previous investigations using a cast support showing that there is an optimized permselectivity to achieve the highest water flux for a given support structure [58]. This finding indicates that along with the support structure, the permeability-selectivity trade-off of the selective layer will play a role in membrane design for FO and PRO.

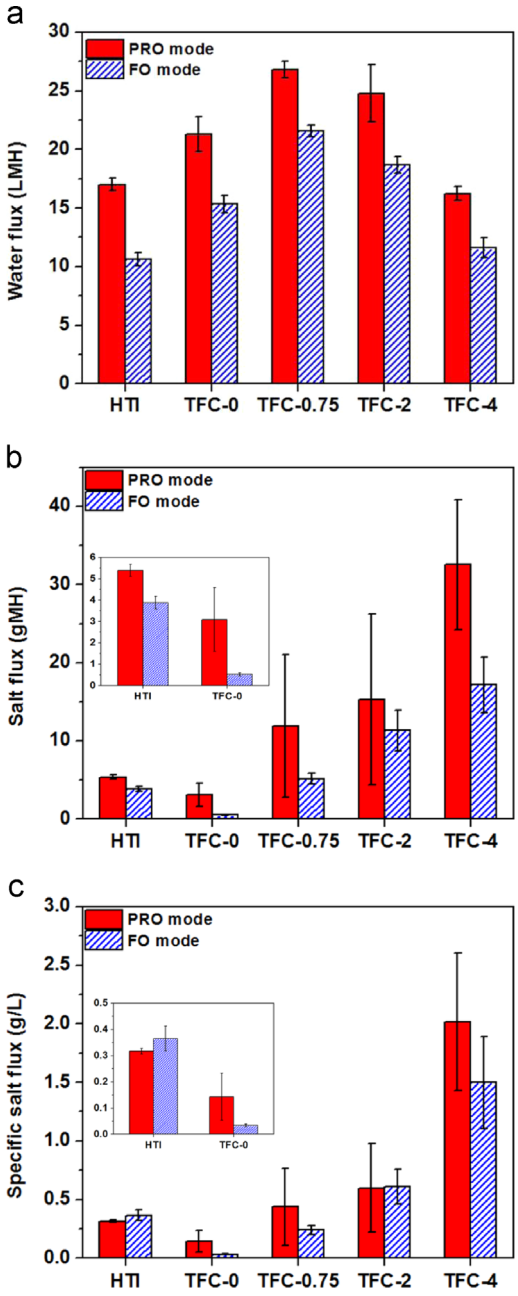


**Fig. 5.** Membrane performance in osmotic flux tests: (a) water flux. (b) Reverse salt flux. The inset shows the reverse salt flux of HTI and TFC-0 with the scale enhanced. (c) Specific salt flux. The inset shows the specific salt flux of HTI and TFC-0 with the scale enhanced. Experimental conditions: $20 \pm 1$ °C; 1.0 M NaCl as the draw solution; DI water as the feed solution; cross-flow velocities of 13.18 cm/s on both sides of the membrane (Re∼600).

Compared to commercial HTI membrane, our TFC membranes generally yield equal or higher water flux in both modes while salt flux varies. Our membrane with the highest water flux performance, TFC-0.75, showed 1.5 × higher water flux in PRO mode, and 2 × higher in FO mode. In terms of reverse salt flux, our IP-TFC membrane (TFC-0) is 2 × lower than HTI in PRO mode and 10 × lower in FO mode. This is not surprising given that "tight polyamide" is typically more selective than cellulose acetate. TFCs based on CAIP (TFC-0.75, 2, and 4) with intentionally "loose polyamide", though, showed 2–7 fold higher reverse salt flux than the HTI in PRO mode and 1–3 fold higher in FO mode.

Regardless of the permselectivity, each TFC membrane exhibited a high water flux relative to the HTI CA membrane. This result

**Table 4**
Performances of TFC EO membranes based on nanofibers and conventional phase-inversion casting films.

| | Sample | Feed solution | Draw solution | Water flux (LMH) | Salt flux (gMH) | Specific salt flux (g/L) | Reference |
|---|---|---|---|---|---|---|---|
| **Nanofiber supported TFCs** | | | | | | | |
| **PRO mode** | **TFC-0** | DI water | 1.0 M NaCl | 21 | 3.1 | 0.14 | This work |
| | **TFC-0.75** | DI water | 1.0 M NaCl | 27 | 11.9 | 0.44 | This work |
| | **PSu** | DI water | 1.5 M NaCl | 24 | 8.63 | 0.36 | [20] |
| | **TFC-2#** | DI water | 1.0 M NaCl | 47.6 | 21.6 | 0.45 | [36] |
| | **PAN** | DI water | 1.5 M NaCl | 52 | 3.5 | 0.06 | [37] |
| **FO mode** | **TFC-0** | DI water | 1.0 M NaCl | 15 | 0.5 | 0.03 | This work |
| | **TFC-0.75** | DI water | 1.0 M NaCl | 21 | 5.2 | 0.24 | This work |
| | **TFC-2#** | DI water | 1.0 M NaCl | 28.0 | 12.9 | 0.46 | [36] |
| | **PAN** | DI water | 1.5 M NaCl | 29 | 8.7 | 0.29 | [37] |
| **Conventional phase-inversion casting film based TFC** | | | | | | | |
| **PRO mode** | **TFC-EO** | DI water | 1.5 M NaCl | 21.9 | 0.8 | 0.04 | [33] |
| **FO mode** | **TFC-EO** | DI water | 1.5 M NaCl | 6.0 | 0.7 | 0.11 | [33] |

indicates that while the selective layer permselectivity matters, structural parameter is still a strong indicator of membrane water flux performance. Using the model presented in Eq. (1), the structural parameter of the TFC-0 membrane is estimated to be approximately 190 um. This is less than half of the commercial HTI membrane.

Specific salt flux, $J_s/J_w$, is a metric that is used to determine the amount of draw solute loss per unit of water produced [59,60]. It is used to compare overall membrane performance when different membranes and/or draw solutes are used. Lower $J_s/J_w$ is desirable to prevent the loss of draw solutes in FO and help to minimize ICP in PRO. As can be seen in Fig. 5(c), $J_s/J_w$ significantly increased with increasing Ac concentration largely due to considerable increase in reverse salt flux. Compared to HTI, our TFC-0 showed half the specific salt flux in PRO mode and one-twelfth in the FO mode.

The CAIP membranes showed different behavior. As the Ac concentration was increased to 0.75%, the water flux increased substantially. However, higher Ac concentrations yielded less selective membranes and decreasing water flux because of lost osmotic pressure and concentration polarization. While an optimum water flux occurs at 0.75% Ac, both salt flux and specific salt flux increases as well. This means as the membrane becomes less selective, water flux is increasing at the same time that salt flux is increasing by larger amount. Eventually that salt flux becomes so high that it reduces the osmotic driving force. It should be noted, however, that even with a 2–7 fold higher salt flux, the CAIP membranes exhibited matched or better water flux than the HTI in both the FO and PRO modes.

These results indicate that higher salt flux, such as those seen with the CAIP membranes, do not necessarily impair water flux. The low structural parameter of these membranes offsets the problems with increased salt flux (internal concentration polarization, lost osmotic driving force) to a degree. In the FO mode, salt is lost through the membrane, but a low $S$ allows for better utilization of the osmotic pressure that is available. In the PRO mode, salt flux induces ICP, but a low $S$ values mitigates ICP.

Along with comparison to a commercial benchmark, the nylon 6,6 nanofiber supported TFC membranes (TFC-0 and TFC-0.75) were also compared to other nanofiber based TFC EO membranes [20,36,37] as well as a TFC membrane based on nylon 6,6 phase-inversion casting film [33]. As seen in Table 4, our TFC membranes exhibited comparable water flux to other nanofiber based TFC membranes especially in FO mode. In addition, our membranes generally have matched or even lower specific salt fluxes in both orientations. Compared to nylon 6,6 MF casting support based TFC, this nanofiber based TFC membranes showed significant improved water flux especially in FO mode, which might be attributed to the intrinsically low structural parameter characteristics of the nanofiber support. Interestingly enough, our TFC-0 even showed a lower specific salt flux than cast film based TFC in FO mode, considering nanofiber based TFC membranes are generally weaker and more prone to salt cross over than conventional casting-film based counterpart.

## 4. Conclusions

This study investigates the use of hydrophilic nylon 6,6 nanofiber supported TFC membranes for use in engineered osmosis. These membranes were fabricated using a cosolvent assisted interfacial polymerization method to achieve different water permeance and salt selectivity. Evaluating these different membranes provided a more fundamental understanding of structure–performance relationships in low structural parameter osmotic membranes. While exhibiting low structural parameters reported in the literature, these membranes exhibited a remarkably high tolerance for salt crossover from the draw solution. While some of our membranes exhibited very low salt flux compared to the HTI cellulose acetate membrane, even those with very high salt flux, matched or outperformed the HTI cellulose acetate membrane in terms of water flux (an important metric for PRO performance). This was attributed to the low structural parameter of the membranes which mitigated internal CP. We believe that such performance and tolerance to low selectivity make this membrane an excellent candidate for further exploration in EO, especially in applications where reverse salt flux is not a key factor of performance.

## Acknowledgments

We acknowledge funding from the U.S. Environmental Protection Agency (#R834872), the Department of Energy (DE-EE00003226), the National Science Foundation (CBET #1160098), and the 3M Nontenured Faculty Award. We thank Hydration Technologies Innovations for providing membranes for this work.

## References

[1] R.L. McGinnis, M. Elimelech, Global challenges in energy and water supply: the promise of engineered osmosis, Environ. Sci. Technol. 42 (2008) 8625–8629.
[2] T.Y. Cath, A.E. Childress, M. Elimelech, Forward osmosis: principles, applications, and recent developments, J. Membr. Sci. 281 (2006) 70–87.
[3] K.L. Lee, R.W. Baker, H.K. Lonsdale, Membranes for power-generation by pressure-retarded osmosis, J. Membr. Sci. 8 (1981) 141–171.
[4] J. Kessler, C. Moody, Drinking water from sea water by forward osmosis, Desalination 18 (1976) 297–306.

[5] J.R. McCutcheon, M. Elimelech, Desalination by ammonia–carbon dioxide forward osmosis: influence of draw and feed solution concentrations on process performance, J. Membr. Sci. 278 (2006) 114–123.
[6] C.R. Martinetti, A.E. Childress, T.Y. Cath, High recovery of concentrated RO brines using forward osmosis and membrane distillation, J. Membr. Sci. 331 (2009) 31–39.
[7] T.Y. Cath, N.T. Hancock, C.D. Lundin, C. Hoppe-Jones, J.E. Drewes, A multi-barrier osmotic dilution process for simultaneous desalination and purification of impaired water, J. Membr. Sci. 362 (2010) 417–426.
[8] S. Loeb, The Osmotic Power Plant, 1996 31st Intersociety Energy Conversion Engineering Conference, vol. 1, 1976, p. 51.
[9] S. Loeb, Energy production at the Dead Sea by pressure-retarded osmosis: challenge or chimera? Desalination 120 (1998) 247–262.
[10] S. Loeb, One hundred and thirty benign and renewable megawatts from Great Salt Lake? The possibilities of hydroelectric power by pressure-retarded osmosis, Desalination 141 (2001) 85–91.
[11] S. Loeb, Large-scale power production by pressure-retarded osmosis, using river water and sea water passing through spiral modules, Desalination 143 (2002) 115–122.
[12] E. Beaudry, K. Lampi, Membrane technology for direct-osmosis concentration of fruit juices, Food Technol. 44 (6) (1990) 121.
[13] K.B. Petrotos, P. Quantick, H. Petropakis, A study of the direct osmotic concentration of tomato juice in tubular membrane – module configuration. I. The effect of certain basic process parameters on the process performance, J. Membr. Sci. 150 (1998) 99–110.
[14] K.B. Petrotos, H.N. Lazarides, Osmotic concentration of liquid foods, J. Food Eng. 49 (2001) 201–206.
[15] N.Y. Yip, A. Tiraferri, W.A. Phillip, J.D. Schiffman, M. Elimelech, High performance thin-film composite forward osmosis membrane, Environ. Sci. Technol. 44 (2010) 3812–3818.
[16] R. Wang, L. Shi, C.Y. Tang, S. Chou, C. Qiu, A.G. Fane, Characterization of novel forward osmosis hollow fiber membranes, J. Membr. Sci. 355 (2010) 158–167.
[17] A. Tiraferri, N.Y. Yip, W.A. Phillip, J.D. Schiffman, M. Elimelech, Relating performance of thin-film composite forward osmosis membranes to support layer formation and structure, J. Membr. Sci. 367 (2011) 340–352.
[18] Q. Saren, C.Q. Qiu, C.Y. Tang, Synthesis and characterization of novel forward osmosis membranes based on layer-by-layer assembly, Environ. Sci. Technol. 45 (2011) 5201–5208.
[19] J. Wei, C. Qiu, C.Y. Tang, R. Wang, A.G. Fane, Synthesis and characterization of flat-sheet thin film composite forward osmosis membranes, J. Membr. Sci. 372 (2011) 292–302.
[20] N.-N. Bui, M.L. Lind, E.M.V. Hoek, J.R. McCutcheon, Electrospun nanofiber supported thin film composite membranes for engineered osmosis, J. Membr. Sci. 385–386 (2011) 10–19.
[21] S. Chou, L. Shi, R. Wang, C.Y. Tang, C. Qiu, A.G. Fane, Characteristics and potential applications of a novel forward osmosis hollow fiber membrane, Desalination 261 (2010) 365–372.
[22] S. Chou, R. Wang, L. Shi, Q. She, C. Tang, A.G. Fane, Thin-film composite hollow fiber membranes for pressure retarded osmosis (PRO) process with high power density, J. Membr. Sci. 389 (2012) 25–33.
[23] R.J. Petersen, Composite reverse osmosis and nanofiltration membranes, J. Membr. Sci. 83 (1993) 81–150.
[24] J.R. McCutcheon, M. Elimelech, Influence of concentrative and dilutive internal concentration polarization on flux behavior in forward osmosis, J. Membr. Sci. 284 (2006) 237–247.
[25] J.R. McCutcheon, R.L. McGinnis, M. Elimelech, A novel ammonia–carbon dioxide forward (direct) osmosis desalination process, Desalination 174 (2005) 1–11.
[26] R.W. Baker, Membrane Technology and Applications, Wiley, West Sussex, 2004.
[27] I.M. Hutten, Handbook of Nonwoven Filter Media, 1st ed., Butterworth-Heinemann, Oxford; Burlington, MA, 2007.
[28] M. Mulder, Basic Principles of Membrane Technology, Dordrecht; Boston, 2nd ed., Kluwer Academic, 1996.
[29] G.D. Mehta, S. Loeb, Internal polarization in the porous substructure of a semipermeable membrane under pressure-retarded osmosis, J. Membr. Sci. 4 (1978) 261–265.
[30] G.D. Mehta, Further results on the performance of present-day osmotic membranes in various osmotic regions, J. Membr. Sci. 10 (1982) 3–19.
[31] G.T. Gray, J.R. McCutcheon, M. Elimelech, Internal concentration polarization in forward osmosis: role of membrane orientation, Desalination 197 (2006) 1–8.
[32] J.R. McCutcheon, M. Elimelech, Influence of membrane support layer hydrophobicity on water flux in osmotically driven membrane processes, J. Membr. Sci. 318 (1–2) (2008) 458–466.
[33] L. Huang, N.-N. Bui, M.T. Meyering, T.J. Hamlin, J.R. McCutcheon, Novel hydrophilic nylon 6,6 microfiltration membrane supported thin film composite membranes for engineered osmosis, J. Membr. Sci. 437 (2013) 141–149.
[34] X. Song, Z. Liu, D.D. Sun, Nano gives the answer: breaking the bottleneck of internal concentration polarization with a nanofiber composite forward osmosis membrane for a high water production rate, Adv. Mater. 23 (2011) 3256–3260.
[35] X. Song, Z. Liu, D.D. Sun, Energy recovery from concentrated seawater brine by thin-film nanofiber composite pressure retarded osmosis membranes with high power density, Energy Environ. Sci. 6 (2013) 1199–1210.
[36] M. Tian, C. Qiu, Y. Liao, S. Chou, R. Wang, Preparation of polyamide thin film composite forward osmosis membranes using electrospun polyvinylidene fluoride (PVDF) nanofibers as substrates, Sep. Purif. Technol. 118 (2013) 727–736.
[37] N.-N. Bui, J.R. McCutcheon, Hydrophilic nanofibers as new supports for thin film composite membranes for engineered osmosis, Environ. Sci. Technol. 47 (2013) 1761–1769.
[38] C. Kong, M. Kanezashi, T. Yamomoto, T. Shintani, T. Tsuru, Controlled synthesis of high performance polyamide membrane with thin dense layer for water desalination, J. Membr. Sci. 362 (2010) 76–80.
[39] M.M. Mannarino, R. Katsumata, G.C. Rutledge, Structural, mechanical, and tribological properties of electrospun poly(hexamethylene adipamide) fiber mats, Wear 305 (2013) 58–68.
[40] A. Huber, A. Pickett, K.M. Shakesheff, Reconstruction of spatially orientated myotubes in vitro using electrospun, parallel microfibre arrays, Eur. Cells Mater. 14 (2007) 56–63.
[41] C.J. Buchko, L.C. Chen, Y. Shen, D.C. Martin, Processing and microstructural characterization of porous biocompatible protein polymer thin films, Polymer 40 (1999) 7397–7407.
[42] K. Behler, M. Havel, Y. Gogotsi, New solvent for polyamides and its application to the electrospinning of polyamides 11 and 12, Polymer 48 (2007) 6617–6621.
[43] K. Yoon, B.S. Hsiao, B. Chu, Formation of functional polyethersulfone electrospun membrane for water purification by mixed solvent and oxidation processes, Polymer 50 (2009) 2893–2899.
[44] Z.H. Tang, C.Q. Qiu, J.R. McCutcheon, K. Yoon, H.Y. Ma, D.F. Fang, E. Lee, C. Kopp, B.S. Hsiao, B. Chu, Design and fabrication of electrospun polyethersulfone nanofibrous scaffold for high-flux nanofiltration membranes, J. Polym. Sci. Pt. B-Polym. Phys. 47 (2009) 2288–2300.
[45] L. Huang, N.N. Bui, S.S. Manickam, J.R. McCutcheon, Controlling electrospun nanofiber morphology and mechanical properties using humidity, J. Polym. Sci. Part B: Polym. Phys. 49 (2011) 1734–1744.
[46] L. Huang, S.S. Manickam, J.R. McCutcheon, Increasing strength of electrospun nanofiber membranes for water filtration using solvent vapor, J. Membr. Sci. 436 (2013) 213–220.
[47] J. Arena, B. McCloskey, B. Freeman, J.R. McCutcheon, Surface modification of anisotropic thin film composite membrane support layers with polydopamine to facilitate water transport in pressure retarded osmosis, J. Membr. Sci. 375 (2011) 55–62.
[48] A. Tiraferri, N.Y. Yip, A.P. Straub, S. Romero-Vargas Castrillon, M. Elimelech, A method for the simultaneous determination of transport and structural parameters of forward osmosis membranes, J. Membr. Sci. 444 (2013) 523–538.
[49] S.S Manickam, J.R. McCutcheon, Characterization of polymeric nonwovens using porosimetry, porometry and X-ray computed tomography, J. Membr. Sci. 407 (2012) 108–115.
[50] A.K. Ghosh, E.M.V. Hoek, Impacts of support membrane structure and chemistry on polyamide–polysulfone interfacial composite membranes, J. Membr. Sci. 336 (2009) 140–148.
[51] P.S. Singh, S.V. Joshi, J.J. Trivedi, C.V. Devmurari, A.P. Rao, P.K. Ghosh, Probing the structural variations of thin film composite RO membranes obtained by coating polyamide over polysulfone membranes of different pore dimensions, J. Membr. Sci. 278 (2006) 19–25.
[52] V. Freger, Kinetics of film formation by interfacial polycondensation, Langmuir 21 (2005) 1884–1894.
[53] Z. Ma, M. Kotaki, S. Ramakrishna, Electrospun cellulose nanofiber as affinity membrane, J. Membr. Sci. 265 (2005) 115–123.
[54] S.-S. Choi, Y.S. Lee, C.W. Joo, S.G. Lee, J.K. Park, K.-S. Han, Electrospun PVDF nanofiber web as polymer electrolyte or separator, Electrochim. Acta 50 (2004) 339–343.
[55] N. Widjojo, T.-S. Chung, M. Weber, C. Maletzko, V. Warzelhan, The role of sulphonated polymer and macrovoid-free structure in the support layer for thin-film composite (TFC) forward osmosis (FO) membranes, J. Membr. Sci. 383 (2011) 214–223.
[56] G. Han, T.-S. Chung, M. Toriida, S. Tamai, Thin-film composite forward osmosis membranes with novel hydrophilic supports for desalination, J. Membr. Sci. (2012).
[57] S. Zhang, F. Fu, T.-S. Chung, Substrate modifications and alcohol treatment on thin film composite membranes for osmotic power, Chem. Eng. Sci. 87 (2013) 40–50.
[58] N.Y. Yip, A. Tiraferri, W.A. Phillip, J.D. Schiffrnan, L.A. Hoover, Y.C. Kim, M. Elimelech, Thin-film composite pressure retarded osmosis membranes for sustainable power generation from salinity gradients, Environ. Sci. Technol. 45 (2011) 4360–4369.
[59] W.A. Phillip, J.S. Yong, M. Elimelech, Reverse draw solute permeation in forward osmosis: modeling and experiments, Environ. Sci. Technol. 44 (2010) 5170–5176.
[60] N.T. Hancock, T.Y. Cath, Solute coupled diffusion in osmotically driven membrane processes, Environ. Sci. Technol. 43 (2009) 6769–6775.